Atmospheric Environment, Volume 166, 2017, Pages 498-509
DOI:10.1016/j.atmosenv.2017.07.047

Influence of Northeast Monsoon Cold Surges on Air Quality in Southeast Asia

M. J. Ashfold[a,*], M. T. Latif[b,c], A. A. Samah[d], M. I. Mead[e], N. R. P. Harris[e]

[a] School of Environmental and Geographical Sciences, University of Nottingham Malaysia Campus, 43500 Semenyih, Selangor, Malaysia

[b] School of Environmental and Natural Resource Sciences, Faculty of Science and Technology, Universiti Kebangsaan Malaysia, 43600 Bangi, Selangor, Malaysia

[c] Institute for Environment and Development (Lestari), Universiti Kebangsaan Malaysia, 43600 Bangi, Selangor, Malaysia

[d] Institute of Ocean and Earth Sciences, University of Malaya, 50603 Kuala Lumpur, Malaysia

[e] Centre for Atmospheric Informatics and Emissions Technology, Cranfield University, Cranfield, MK43 0AL, United Kingdom

***** *Corresponding author: Matthew J. Ashfold (matthew.ashfold@nottingham.edu.my; +6 03 8725 3434)*

Abstract

Ozone (O_3) is an important ground-level pollutant. O_3 levels and emissions of O_3 precursors have increased significantly over recent decades in East Asia and export of this O_3 eastward across the Pacific Ocean is well documented. Here we show that East Asian O_3 is also transported southward to tropical Southeast (SE) Asia during the Northeast Monsoon (NEM) season (defined as November to February), and that this transport pathway is especially strong during 'cold surges'. Our analysis employs reanalysis data and measurements from surface sites in Peninsular Malaysia, both covering 2003-2012, along with trajectory calculations. Using a cold surge index (northerly winds at 925 hPa averaged over 105-110°E, 5°N) to define sub-seasonal strengthening of the NEM winds, we find the largest changes in a region covering much of the Indochinese Peninsular and surrounding seas. Here, the levels of O_3 and another key pollutant, carbon monoxide, calculated by the Monitoring

Atmospheric Composition and Climate (MACC) Reanalysis are on average elevated by, respectively, >40% (~15 ppb) and >60% (~80 ppb) during cold surges. Further, in the broader region of SE Asia local afternoon exceedances of the World Health Organization's air quality guideline for O_3 (100 µg m^{-3}, or ~50 ppb, averaged over 8 hours) largely occur during these cold surges. Day-to-day variations in available O_3 observations at surface sites on the east coast of Peninsular Malaysia and in corresponding parts of the MACC Reanalysis are similar, and are clearly linked to cold surges. However, observed O_3 levels are typically ~10-20 ppb lower than the MACC Reanalysis. We show that these observations are also subject to influence from local urban pollution. In agreement with past work, we find year-to-year variations in cold surge activity related to the El Nino-Southern Oscillation (ENSO), but this does not appear to be the dominant influence of ENSO on atmospheric composition in this region. Overall, our study indicates that the influence of East Asian pollution on air quality in SE Asia during the NEM could be at least as large as the corresponding, well-studied spring-time influence on North America. Both an enhanced regional observational capability and chemical modelling studies will be required to fully untangle the importance of this long-range influence relative to local processes.

Keywords: Air quality; Ozone; Pollution; Northeast Monsoon; Southeast Asia

Highlights

- Cold surges in November-February transport East Asian pollution to Southeast Asia
- Regional exceedances of the WHO's O_3 guideline often occur during cold surges
- Surface measurement sites in region also influenced by local sources of pollution
- More observations in region and chemical modelling needed for further understanding

1. Introduction

Ground-level ozone (O_3) has important impacts on human health (Lelieveld et al., 2015), and these impacts are likely to be large throughout the 21st century (Silva et al., 2016). In the tropical boundary

layer there are year-to-year variations in O_3 linked to the El Nino-Southern Oscillation (ENSO), which modifies chemical and transport processes, and drives changes in emissions of O_3 precursors (e.g. Inness et al., 2015; Hou et al., 2016). However, Ziemke et al. (2015) reported that variability in tropical tropospheric O_3 is primarily driven by shorter timescale (non-ENSO) phenomena. One such form of shorter-timescale variation is East Asian 'cold surges', characterised by periodic strengthening of the prevailing north-easterly winds during the northern hemisphere (NH) winter monsoon (or Northeast Monsoon, NEM), that have been studied for decades in a meteorological context (e.g. Chang et al., 1979; Zhang et al., 1997). However, while past work (e.g. Liu et al., 2003; Wang et al., 2016) has examined the influence of cold surges on atmospheric composition away from the tropics, their importance for the tropics has received little attention.

This tropical impact could be large as during NH winter high levels of mid-latitude pollution found in East Asia (e.g. Stein et al., 2014) are matched with unusually strong northerly winds towards the equator. There is clearly great potential for significant transport of pollution to the deep tropics within this particular range of longitudes, and this is particularly true during cold surge events. For example, using trajectory calculations and observations for one NH winter Ashfold et al. (2015) showed that cold surges could rapidly (over a few days) transport polluted air masses from East Asia to tropical Southeast (SE) Asia. Oram et al. (unpublished results) present further measurements and model results which demonstrate the likely importance of this mechanism for transporting large quantities of short-lived chlorinated compounds, with the capacity to deplete stratospheric O_3, from East Asian emission sources to the tropics.

Yet the spatial and temporal extent to which these cold surges affect air quality, including O_3 levels, in SE Asia is not clear. It is well known that pollution originating in East Asia and transported eastward leads to elevated O_3 levels above the North Pacific Ocean and in North America (e.g. Wild and Akimoto, 2001; Liu et al., 2003; Zhang et al., 2008; Cooper et al., 2010; Lin et al., 2012; Lin et al., 2014; Verstraeten et al., 2015), and so an equivalent impact in SE Asia linked to cold surges might be expected. Such an impact is hinted at by Ashfold et al. (2015) who showed that cold surges could increase O_3, as well as carbon monoxide (CO), another harmful gas that is often used as a marker for

anthropogenic pollution, to approximately double the levels typically found in the 'clean' background atmosphere over the relatively short (~weeks-months) period covered by their analysis.

In this study we investigate more thoroughly the relationship between cold surges and SE Asian air quality, with a particular focus on O_3, using longer-term datasets. We describe various aspects of our methodology in Section 2. In Section 3.1 we provide a climatological background, and in Section 3.2 we characterize our cold surge index. Then in Section 3.3 we 1) use this index to explore air quality composites for cold surge and non-cold surge conditions, 2) use dispersion model calculations to further investigate the link between cold surges and high levels of pollution, and 3) consider the importance of cold surges in driving exceedances of air quality thresholds in our study region on a day-to-day basis. In Section 3.4 we compare reanalysis data with observations from surface sites. Our final analysis, in Section 3.5, focuses on whether the known influence of ENSO on cold surge activity is an important driver of year-to-year variations in pollution in SE Asia. Section 4 contains a discussion of our key findings.

2. Data and Methodology

2.1 Reanalysis data

Much of our analysis relies on the Monitoring Atmospheric Composition and Climate (MACC) Reanalysis of atmospheric composition (Inness et al., 2013), which has been used successfully in studies of the tropical atmosphere (e.g. Inness et al., 2015; Ashfold et al., 2015). We extracted O_3, CO and meridional wind (v) data for each November, December, January and February (NDJF) in the 10 year period covered by the dataset (2003-2012). We analyse time-steps at 06:00 and 18:00 Universal Time (UT), or approximately 14:00 and 02:00 local time (LT). We consider a region covering tropical SE Asia (90-125°E, 10°S-20°N), and extracted data with a horizontal resolution of 1.125° longitude by 1.125° latitude, which is the native resolution of the chemical transport model within the reanalysis system. We mostly present data on the 925 hPa pressure level, which is likely to be representative of boundary layer conditions but less influenced by local surface processes than the alternative 1000 hPa

pressure level. Where necessary, we show that the choice of pressure level and time-step is not critical to our conclusions. As well as gridded values, for purposes of comparison with observations, we use bilinear interpolation to obtain MACC Reanalysis data for measurement site locations. Inness et al. (2013) assessed the quality of the MACC Reanalysis through comparisons with independent observations, and found modest negative biases of up to ~20% for O_3 through much of the tropical troposphere, but slight positive biases (i.e. the reanalysis values were higher than the compared ozone sonde values) below ~800 hPa. It is worth noting, however, the relative paucity of observations available for validation in the region of the tropics covered by our study.

We also consider meridional wind data, for the same spatial region, from the ERA-Interim reanalysis (Dee et al., 2011). We extracted a longer record, covering NDJF 1979-2015, at a horizontal resolution of 0.75°, to enable a more thorough analysis of the wind regime in our study area. Bocquet et al. (2015) note that the configuration of the MACC Reanalysis system is similar to that of ERA-Interim, and indeed for our region of interest the winds in the two datasets are alike. For example, in Section 2.2 we describe an index for defining cold surges using meridional winds at 925 hPa, averaged over 105-110°E, at 5°N. Despite being interpolated from grids with different resolutions, the values of this index over the period of the MACC reanalysis (2003-2012) in the two datasets are similar: coefficient of determination, $r^2 = 0.98$ ($p < 0.001$), MACC mean = -5.4 m s^{-1}; ERA-Interim mean = -4.8 m s^{-1}.

2.2 Cold Surge definition

There is no universal definition of a cold surge, with different authors typically using a definition that best suits the geographical scope of their investigation. For example, Zhang et al. (1997) and Huang et al. (2011) studied movement of the Siberian High – a typical feature of cold surge initiation – using definitions based on aspects of sea level pressure and temperature over East Asia. In contrast, Chang et al. (2005) studied the downstream impacts of cold surges on tropical convection and defined a cold surge index using meridional wind at 925 hPa averaged over 110-117.5°E at 15°N. The same authors defined a cold surge event when this index was stronger than -8 m s^{-1}. The definition of Chang et al. (2005) was also adopted by Ooi et al. (2011), Hai et al. (2017) and, with slight modification, by Juneng and Tanggang (2010) in their studies focused on the tropical atmosphere. In our analysis we

also employ the definition of Chang et al. (2005), which we will call V_{15}. As we are interested in changes in composition in the deep tropics, and will make comparisons with air quality measurements collected near 5°N in Peninsular Malaysia (see Section 2.4) we also define a second, similar index - meridional wind at 925 hPa averaged over 105-110°E at 5°N - which we will call V_5. In either case, again in accordance with Chang et al. (2005), we define a cold surge event when $v < -8$ m s^{-1} (i.e. when the magnitude of the northerly wind component is larger than 8 m s^{-1}).

2.3 Dispersion model calculations

To examine transport pathways associated with cold surges and variations in air quality we calculated backward trajectories using the Numerical Atmospheric-dispersion Modelling Environment (NAME; Jones et al., 2007), a Lagrangian particle dispersion model. Owing to the availability of driving meteorological data we focus on calculations covering the final three complete NDJF seasons in the MACC Reanalysis (i.e. November 2009-February 2010 to November 2011-February 2012). For each 3 hour period in these seasons, batches of 60,000 inert backward trajectories were started from a source region covering the horizontal coordinates of the V_5 region (i.e. 105-110°E at 5°N) defined in Section 2.2, and within an altitude range of 0-100 m. The trajectories were calculated over 12 days, and every 15 minutes the location of all trajectories within the lowest 100 m of the model atmosphere was recorded on a grid with a horizontal resolution of 0.5625° longitude by 0.375° latitude. The model output on this grid was converted to an emission sensitivity – a quantitative measure of how sensitive a receptor is to emissions in a grid cell – with units of s m^{-1} (i.e. g m^{-3} / g m^{-2} s^{-1}). In addition to the three seasons noted above, for illustration, we also present similar calculations for two specific days: 13 and 23 January 2009.

The trajectories were calculated using three-dimensional meteorological fields produced by the UK Meteorological Office's Numerical Weather Prediction tool, the Unified Model (UM). These fields are available at 3 hour intervals and have varying spatial resolution. For calculations up to the end of February 2010 they have a horizontal resolution of 0.5625° longitude by 0.375° latitude and 52 vertical levels below ~20 km. For calculations beginning in November 2010 they have a horizontal

grid resolution of ~0.35° longitude by ~0.23° latitude and 59 vertical levels below ~30 km. The sub-grid scale process of turbulence is parameterised in NAME (Morrison and Webster, 2005).

2.4 Surface air quality measurements

For comparison with the MACC Reanalysis we also analyse O_3 and CO data from stations in a network managed by Alam Sekitar Sdn Bhd (ASMA), a company which measures air quality on behalf of the Malaysian Department of Environment (DOE). Covering more than 50 locations in Malaysia around the southern edge of the South China Sea (SCS), the DOE network represents, to our knowledge, the most widespread, long-term record of air quality in tropical SE Asia. Quality control procedures for this network are described by Latif et al. (2014; their section 3.3) and ASMA (2007). Observations from the DOE network have been analysed previously in several studies (e.g. Latif et al., 2016 and references therein). Of importance here, Latif et al. (2014) have shown that even at the designated 'background' station in this network, at Jerantut, there is evidence that local pollution (e.g. from traffic) impacts the available observations. Accordingly, we will consider how useful the DOE data are for studying the impact on air quality of large-scale meteorological processes such as cold surges.

Our analysis of the DOE data focuses on three stations close to the east coast of Peninsular Malaysia, at Kota Bharu (102.247°E, 6.141°N), Kuala Terengganu (103.118°E, 5.308°N) and Kemaman (103.428°E, 4.271°N) (refer to Figure 6 to visualise locations). We believe these stations, lying in the path of cold surges during the NEM, offer the best possibility of observing a cold surge influence on air pollution within the DOE network. For each day considered in the MACC Reanalysis (i.e. in the months of NDJF in the years 2003-2012), we compute 'afternoon' mean measured values by averaging the 8 hourly mean values reported at 11:00-18:00 LT. An 8 hour averaging period is commonly used in air quality regulations for O_3, and we use this fixed 'afternoon' window 1) to enable direct comparison with the 14:00 LT time-step in the MACC Reanalysis and 2) because it typically captures peak O_3 values in the DOE network (see Latif et al., 2012; 2014). To avoid bias where the peak in O_3 is not captured fully owing to missing data, we exclude days in which fewer than 5 of the 8 hourly values are available.

2.5 Multivariate ENSO Index

We use the Multivariate ENSO Index (MEI, https://www.esrl.noaa.gov/psd/enso/mei/; Wolter and Timlin, 1998) data for 1979-2015, which corresponds to the period covered in our analysis of ERA-Interim data. When comparing the overlapping bimonthly MEI values with monthly fields we assume the MEI value is valid for the second month (i.e. the MEI value for December-January is compared with the January field of another dataset), as suggested here: https://www.esrl.noaa.gov/psd/enso/mei/table.html. We also calculate seasonal means for NDJF by averaging the bimonthly MEI values for October-November to January-February. Within the period covered by the MACC Reanalysis (2003-2012) we categorise the three highest (MEI > 0.65) NDJF seasonal mean values as El Nino winters (2004/05, 2006/07, 2009/10) and the three lowest (MEI < -0.88) as La Nina winters (2007/08, 2010/11, 2011/12). This categorisation is consistent with that of Inness et al. (2015).

3. Results

3.1 Seasonal variations in atmospheric composition in SE Asia

To set the context for our analysis, we first examine seasonal differences in SE Asia for selected variables in the MACC Reanalysis. Figure 1 shows a climatology of CO, O_3 and v for NH winter (here using the common definition of the season, DJF) in SE Asia. For comparison, NH summer (JJA) climatologies and the differences between the two seasons for the same variables are also shown. In NH winter the strong (northerly component faster than 6 m s^{-1}) north-easterly monsoon winds over the SCS are an obvious climatological feature. Also in NH winter levels of CO over much of Indochina and the SCS are significantly higher (>100 ppb, or >100%) than in NH summer. The polluted air in this region is likely linked to a combination of biomass burning during the dry season in Indochina (e.g. Reid et al., 2013), longer chemical lifetimes in the winter hemisphere, and the phenomenon we explore in more detail in subsequent sections – the transport by northerly winds of polluted air masses from East Asia towards the tropics. Nearer the equator the situation is more mixed, with seasonal

differences (i.e. DJF-JJA) in equatorial parts of SE Asia typically smaller than ±50 ppb for CO and ±10 ppb for O_3. These smaller seasonal differences arise because there are regularly large near-equatorial sources of pollution during JJA, linked to landscape fires often occurring in parts of Indonesia (e.g. Reid et al., 2012; see the elevated climatological CO levels over Sumatra and southern Borneo in Figure 1). In Section 3.2 we focus on the northerly winds during NH winter, and explore the characteristics of cold surges in the context of this study. We then go on, in Section 3.3, to investigate the importance of pollution episodes in SE Asia linked to these cold surges.

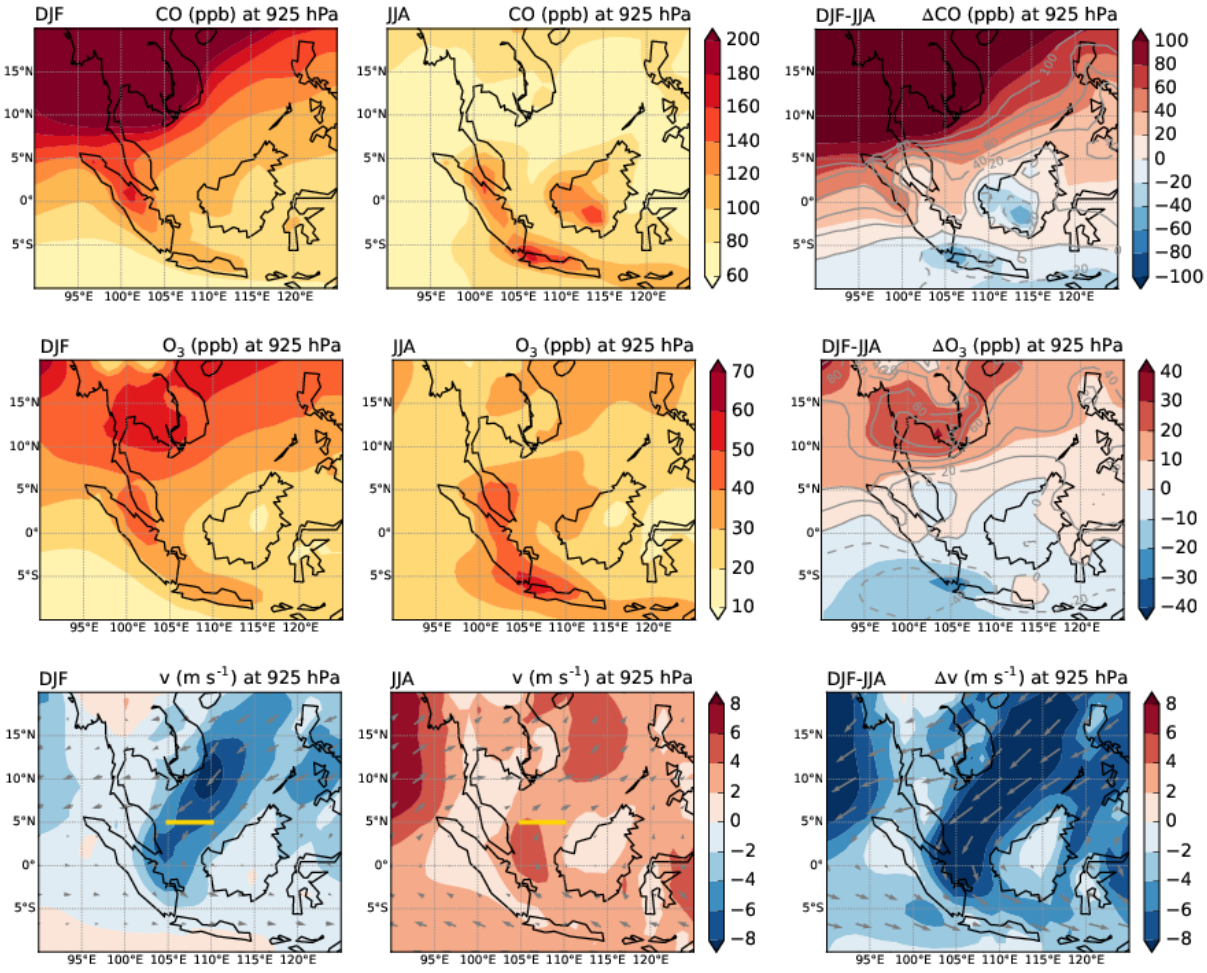

Figure 1: MACC Reanalysis CO (top), O_3 (middle) and meridional wind (bottom), all at 925 hPa, for DJF (left), JJA (centre) and DJF-JJA (right). The MACC data are averaged over 10 years (2003-2012). In the difference plots for CO and O_3 the shading shows absolute differences, and the labelled grey contours show percentage differences. The line over which the V_5 cold surge index, outlined in Section 2.2 and used in subsequent analyses, is calculated is marked in gold in the v panels.

3.2 NE monsoon winds and cold surges

In this section we examine the nature of changes in the northerly winds in the SCS during NH winter, with an emphasis on 'cold surges' as defined in Section 2.2. Considering month-by-month changes, Figure 2 shows that northerly winds in the SCS are generally strongest in December and January. The location of the strongest wind moves south along with the monsoon trough (approximately indicated by the transition from northerly to southerly winds; Reid et al., 2012) through the winter, so that the V_{15} cold surge index is strongest in December and weakens considerably by February, whereas V_5 is relatively weak in November and strengthens to a maximum in January. Clearly different measures of northerly winds will lead to somewhat different results, but overall we find that our key conclusions are not reliant on the choice of V_{15} or V_5. We will focus on V_5 for our subsequent analysis, but given the strength of V_{15} during November (also see Zhang et al., 1997) we analyse NDJF as the relevant 'seasonal' period for cold surges rather than the typical DJF NH winter season.

Beyond the climatological situation, we will consider variability occurring over both day-to-day and year-to-year timescales. With respect to day-to-day variations, the red line in Figure 2 also shows, using the ENSO-neutral NH winter of 2008/09 as an illustrative example, that the strength of monsoon winds (as measured by V_5) during NDJF vary markedly around the average condition, with a clear illustration of a strong (V_5 = -10-12 m s^{-1}) cold surge in early-to-mid January 2009.

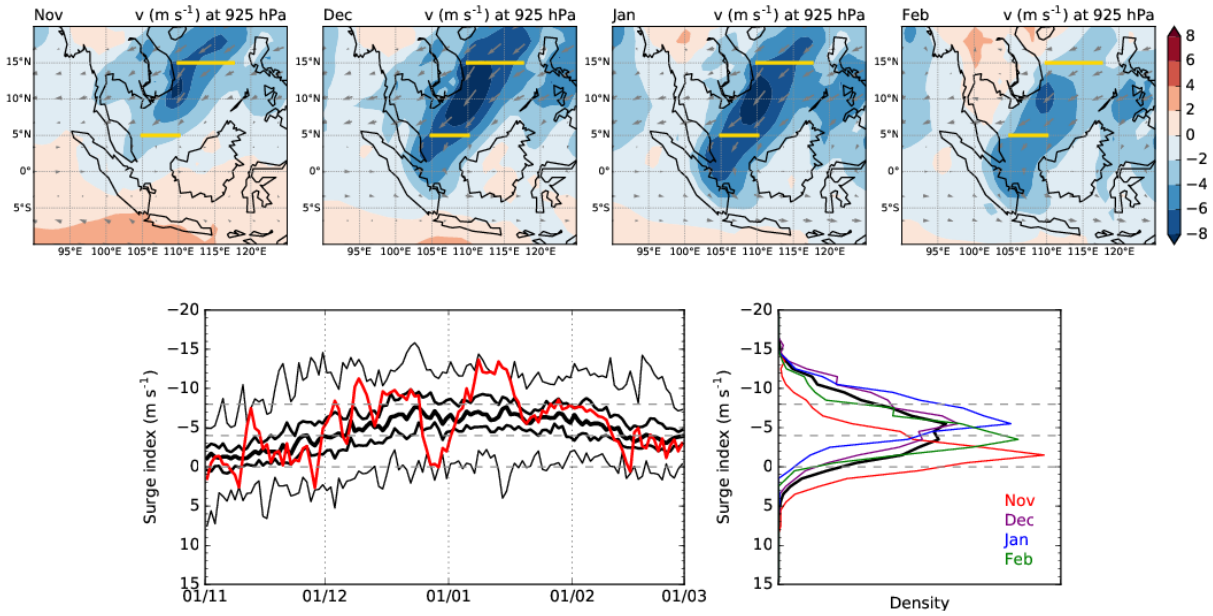

Figure 2: For November-February, the top row shows monthly mean maps of meridional wind (shading) and wind vectors from the MACC Reanalysis. The lines over which two cold surges indices, V_5 and V_{15}, are calculated are marked in gold. In the bottom row, the left panel shows daily mean values of V_5 from November 1 to February 28, with black lines denoting minimum, 25th, 50th and 75th percentile, and maximum values of the 37 years (1979-2015) of ERA Interim data considered. The red line shows NDJF 2008/09 as an example. The right panel shows corresponding monthly (November=red, December=purple, January=blue, February=green) and seasonal (black) mean PDFs of V_5. In both lower panels the V_5 stratifications used in subsequent analyses are marked with dashed grey lines.

For further analysis we consider three stratifications of northerly wind. Similarly to Chang et al. (2005) we define 'cold surges' as $V_5 < -8$ m s^{-1}. We also define 'weak' winds as $V_5 > -4$ m s^{-1}. Winds between these two limits (i.e. $-8 < V_5 < -4$ m s^{-1}) are closer to average. On a day-to-day basis through the 37 years of the ERA-Interim Reanalysis we find that for V_5, weak winds occur 42.2% of the time, cold surge winds 17.9% of the time, and in between conditions 39.9% of the time. In the MACC Reanalysis the corresponding values are 38.6%, 24.9% and 36.5%.

3.3 Cold surges and atmospheric composition

Using these three stratifications of northerly winds we now investigate variations in CO and O_3 in the MACC Reanalysis dataset. Figure 3 presents composites of CO, O_3 and v for all days in the 'cold surge' and 'weak wind' categories defined above, as measured by the V_5 index, along with the difference between these two composites. There are, by definition, significant differences in v, which are accompanied by large differences in atmospheric composition. In a region covering much of the Indochinese Peninsular and surrounding seas CO and O_3 mixing ratios are elevated by, respectively, >60% (~80 ppb) and >40% (~15 ppb), during cold surge conditions. Repeating this analysis using the V_{15} index leads to similar patterns and conclusions, though the regions of maximum enhancements are further from the equator (not shown). This analysis supports the general case for a significant influence on variations in atmospheric composition in SE Asia by pollution within air masses transported from outside the tropics.

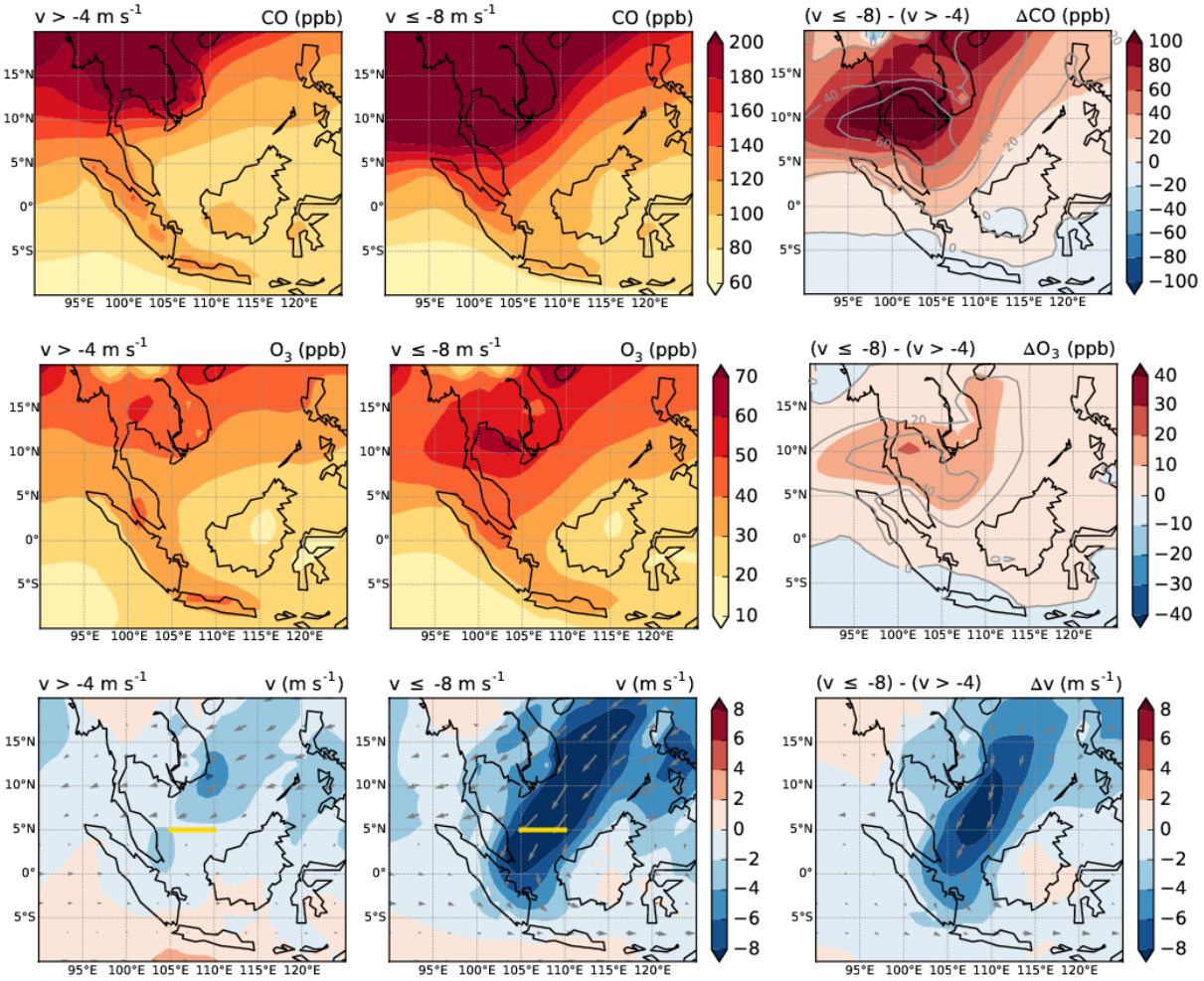

Figure 3: Composites for weak northerly winds (V_5 index > -4 m s^{-1}, left column) and cold surge periods (V_5 index < -8 m s^{-1}, centre) and the difference between the two (right column) for CO (top), O_3 (middle) and v (bottom). The line over which V_5 is calculated is marked in gold in the v panels. In the difference plots for CO and O_3 the shading shows absolute differences, and the labelled grey contours show percentage differences. Constructed from twice daily (06UT and 18UT) MACC Reanalysis data for NDJF in the 10 years of the MACC Reanalysis (i.e. 1203 days). As noted in the main text, 39% of the time steps (929 of 2406) were classed as 'weak wind', 25% (600) were classed as 'cold surge' and 36% (877) were in between (i.e. -8 < v < -4 m s^{-1}).

To explore further the link between transport from outside the tropics and variations in pollution in SE Asia we now examine trajectory calculations. Figure 4 shows composites, presented as emission sensitivities, for backward trajectories started in the V_5 region (see Section 2.3). The composites for the three V_5 stratifications demonstrate clear differences in air mass origin, with weaker V_5 winds linked to air travelling from the subtropical Pacific, and stronger winds (i.e. what we have defined as cold surge conditions) linked to transport of air from the East Asian landmass. In the latter case, the

transport pathway is consistent with the characteristic cold surge circulation pattern discussed by Ashfold et al. (2015), with strong northerly winds in the SCS leading to rapid meridional transport. This analysis suggests the V_5 index is a useful indicator of air mass origin. Next, consider the composites for four stratifications of MACC Reanalysis O_3 in the V_5 region (i.e. at 925 hPa, averaged over 105-110°E at 5°N). In the least polluted stratification (<30 ppb O_3), similar to the weak wind composite, back trajectories largely originate in the subtropical Pacific. In contrast, for the most polluted stratifications (40-50 ppb and >50 ppb O_3), similar to the cold surge composite, the dominant air mass source is the East Asian landmass. Together, this analysis links strong winds in the V_5 region with a cold surge circulation pattern, and with enhanced O_3 pollution in tropical SE Asia.

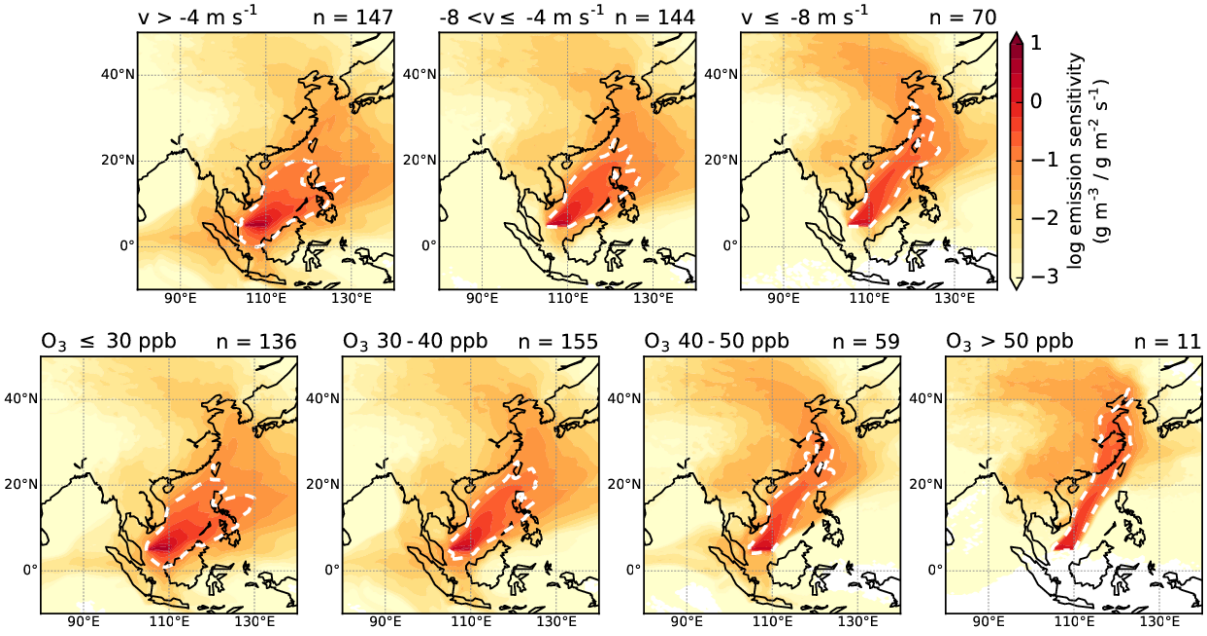

Figure 4: Composites of NAME emission sensitivity calculations for trajectories started in the V_5 region. The top row shows composites for the three V_5 stratifications discussed in Section 3.2 and used in Figure 3. The bottom row shows composites for four stratifications of MACC Reanalysis V_5 O_3 (from <30 ppb, left, to >50 ppb, right; these thresholds are used in Figure 5). The stratification label is given at the top-left of each panel. The number of days (n) contributing to each composite is marked at the top-right of each panel. To aid comparison the 10^{-1} (g m^{-3} / g m^{-2} s^{-1}) emission sensitivity contour is marked with a white dashed line. Constructed from the 361 days in the three complete NDJF seasons (2009/10-2011/12) for which both MACC Reanalysis and NAME data are available. The MACC data are for the 06:00 UT (14:00 LT) time-step, and the NAME trajectories considered were started between 03:00-09:00 UT (11:00-17:00 LT).

We next examine day-to-day variations in northerly winds and O_3 levels, with reference to air quality guidelines. Figure 5 shows the correlation ($r^2 = 0.29$ or $r = -0.54$, $p < 0.001$) between the V_5 index and corresponding O_3 levels (i.e. at 925 hPa, averaged over 105-110°E at 5°N; as used in Figure 4) at 06:00 UT (14:00 LT) for each NDJF day in the ten years covered by the MACC Reanalysis (1203 days in total). Considering the same three stratifications of v, mean (and standard deviation) O_3 values in this southerly part of the SCS are 29.0 (6.3) ppb for weak wind conditions, 34.2 (7.2) ppb for intermediate conditions, and 40.8 (8.3) ppb for cold surge conditions. In this V_5 region the World Health Organization's (WHO) Air Quality Guideline for O_3 (100 µg m^{-3}, i.e. a mixing ratio of ~50 ppb) is exceeded just 5% of the time during NDJF, but 73% of these exceedances occur during cold surge conditions. Exceedances are therefore rare when winds from the north are weaker. The maps in Figure 5 indicate that exceedances of the 50 ppb O_3 threshold in much of this region, particularly in a band centred on 5°N, can be related to cold surge conditions in the V_5 region. Repeating this analysis using a lower O_3 threshold of 40 ppb (also in Figure 5), or a different cold surge definition (V_{15} index, not shown), does not change this overall conclusion.

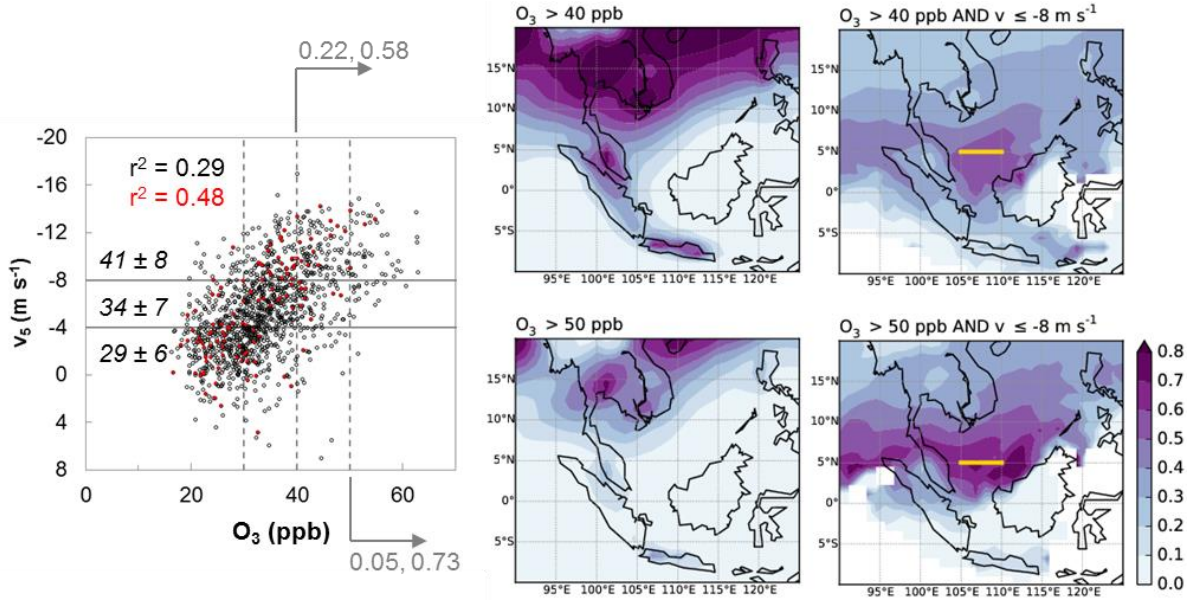

Figure 5: The left panel shows the correlation between MACC V_5 at 06:00 UT (14:00 LT) for each day in NDJF 2003-2012 and O_3 values averaged over the same V_5 region. Illustrative values for NDJF 2008/09 are shown in red. Thresholds of 30, 40 and 50 ppb O_3 (as used in Figure 4) are marked with dashed lines. Mean and standard deviation O_3 values (in ppb) for the three northerly wind stratifications are noted in italics. Coefficient of determination (r^2) values for all NDJF months (black) and for 2008/09 (red) are noted to the top-left; $p < 0.001$ in

both cases. Right, maps showing the fraction (i.e. a number between 0 and 1) of days where the 06:00 UT (14:00 LT) O_3 values are higher than the 40 ppb and 50 ppb thresholds, and the sub-fraction of these days occurring during cold surges ($V_5 < -8$ m s^{-1}). The corresponding fractions related to the scatter plot (i.e. for O_3 averaged over the V_5 region) are marked next to the arrows in grey text.

To illustrate the importance of cold surges in driving day-to-day variations in regional air quality, Figure 6 shows regional patterns of MACC Reanalysis v, CO and O_3 along with NAME emission sensitivities on two selected days, just 10 days apart. Along with the results in Figures 3, 4 and 5, this figure demonstrates the large spatial scale of potential air quality impacts. In the case of 13 January 2009 strong northerly winds and associated polluted air from the East Asian landmass move far south of the equator, reaching the coast of Java (~7°S). The situation on 23 January, when cleaner air originating in the Pacific is found through most of the region, illustrates the marked variations in air quality occurring over periods of days to weeks. In this context, it is also interesting to consider specific locations, and so we compare MACC Reanalysis levels of O_3 on these two days averaged over the V_5 region, and at Kota Bharu, the most northerly of the three surface sites considered in Section 3.4. Consistent with the regional picture, O_3 levels are very different on the two days (44.3 ppb on 13 January and 20.8 ppb on 23 January in the V_5 region; 55.4 ppb and 28.9 at Kota Bharu), but we emphasize that such O_3 levels, and the illustrative days selected, are not particularly unusual within the 10 years of the MACC Reanalysis (respectively the 88^{th} and 4^{th} percentiles in the V_5 region, and the 95^{th} and 12^{th} percentiles at Kota Bharu).

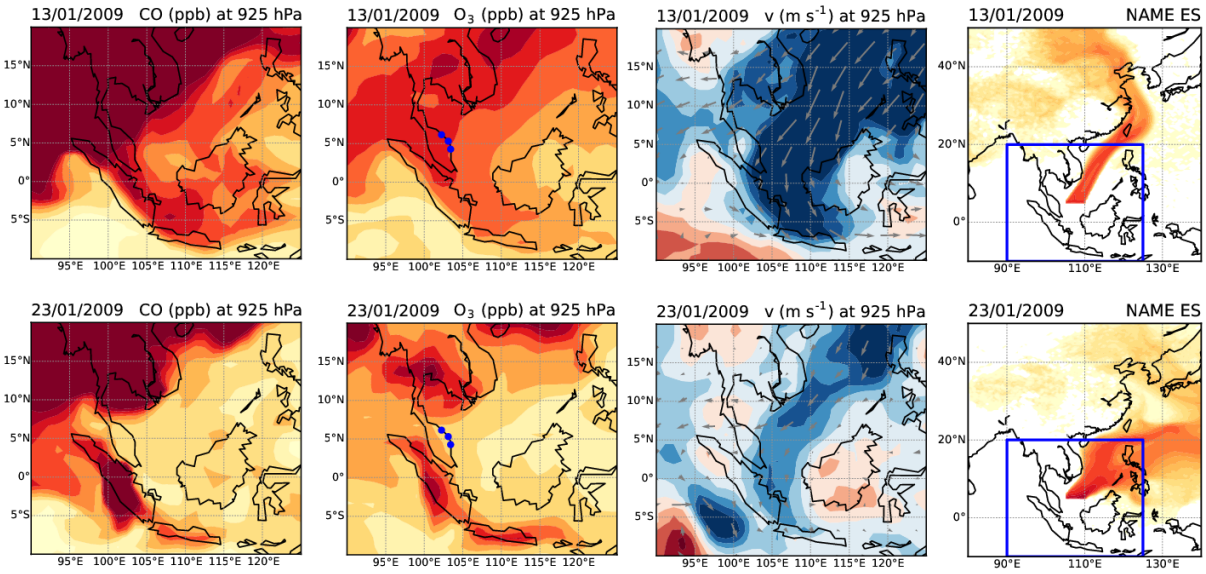

Figure 6: From left to right, examples of MACC Reanalysis data for CO, O_3 and v, and V_5 NAME emission sensitivities (ES), for 13 (top row) and 23 (bottom row) January 2009. The MACC data are at 925 hPa and the 06:00 UT (14:00 LT) time-step. The NAME data are derived from trajectories started between 03:00-09:00 UT (11:00-17:00 LT). The locations of the three surface measurement sites considered in Figure 7 are marked with blue circles in the O_3 panels. The blue box in the NAME panels shows the area considered in the MACC panels. The colour scales are the same as those shown in Figure 3 (MACC data) and Figure 4 (NAME data).

3.4 Comparison of MACC Reanalysis and surface observations

To further examine the day-to-day air quality impacts in this region, we now compare the MACC Reanalysis data with observations from DOE surface sites. This analysis includes all NDJF months in the years 2003-2012. In Figure 7 the calculated daytime means of the DOE observations are compared with corresponding values from the MACC Reanalysis (14:00 LT, 925 hPa, interpolated to horizontal coordinates). The observations and the reanalysis exhibit similar day-to-day variability (r^2 = 0.37–0.48 at the three sites, all $p < 0.001$), suggesting similar processes, linked to cold surges, are captured in both datasets. However, the measured O_3 levels are typically lower than predicted by MACC at all three sites (e.g. overall at Kota Bharu, mean DOE O_3 = 22.3 ppb and mean MACC O_3 = 39.5 ppb). One consequence of this difference is that while exceedances of the WHO's Air Quality Guideline value of 50 ppb are often found (e.g. 50 ppb O_3 is the 87th percentile at Kota Bharu) within the MACC data, such breaches are much rarer (99th percentile) in the observations.

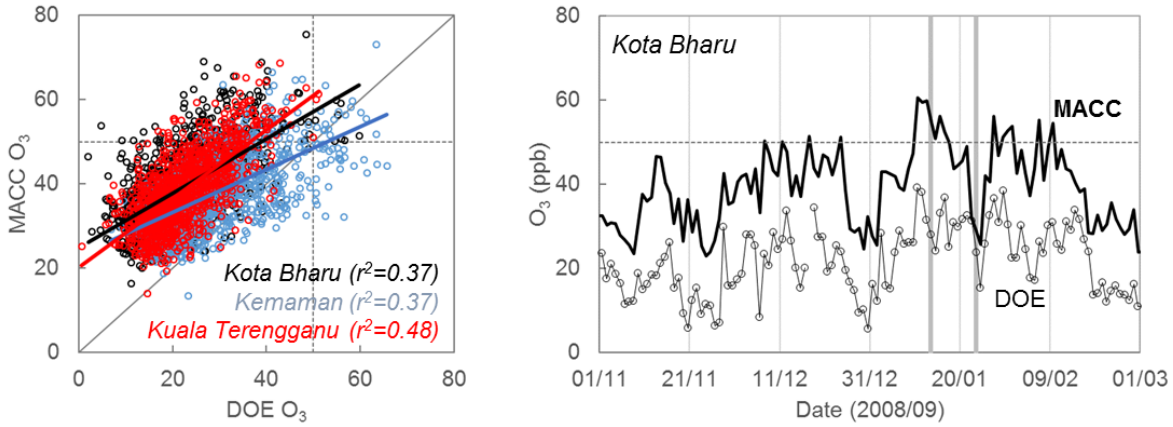

Figure 7: Left, considering all NDJF months in the years 2003-2012, the correlation between MACC and DOE O_3 at the three DOE measurement sites: Kota Bharu (black), Kuala Terengganu (red) and Kemaman (blue). Lines of best-fit are marked and r^2 values are noted; for all three sites $p < 0.001$. The locations of these three surface sites are shown in Figure 5. Right, an illustrative time-series comparison for one NDJF season (November 2008-February 2009) at Kota Bharu. DOE values are 8-hour averages of hourly mean values reported at 11:00-18:00 LT, while MACC values are for 06:00 UT (14:00 LT). The days presented in Figure 5 are marked with solid grey lines. The WHO Air Quality Guideline for 8-hour average O_3 (50 ppb) is shown in both panels with a dashed line.

Why is there such a difference in magnitude between O_3 levels at the DOE sites, and the corresponding MACC values? For consistency with earlier analyses we have used MACC data at 925 hPa, rather than 1000 hPa which may be more suitable for comparison with surface-based observations. However, during local afternoon (14:00 LT), when the boundary layer is expected to be relatively deep (see Samah et al., 2016), there is only a small difference between MACC O_3 values at these two pressure levels (e.g. considering all NDJF in the MACC Reanalysis, for Kota Bharu: $r^2 = 0.94$, $p < 0.001$; 1000 hPa mean = 37.5 ppb, 925 hPa mean = 39.5 ppb). Another small difference is created by comparing instantaneous MACC values with time-averaged observed values. To illustrate, again at Kota Bharu, the average observed O_3 level reported at 14:00 LT (24.3 ppb) is 2 ppb higher than the 'afternoon mean' value calculated over reports from 11:00-18:00 LT (22.3 ppb).

The remaining difference may be linked to the chemical regime in which the observations are made. The DOE sites examined here measure air quality within, or on the edge of, urban centres of several hundred thousand inhabitants, are several km from the coast, and data often exhibit characteristics of

393 the polluted urban atmosphere. Measured daytime CO levels are significantly higher (e.g. mean ~500
394 ppb at Kota Bharu) than are found in the background atmosphere, or at the site locations within the
395 MACC Reanalysis, and some of the lowest measured O_3 values are associated with high levels (10s
396 ppb) of nitrogen oxides. In addition, while there is a strong positive relationship between O_3 and CO
397 in the MACC Reanalysis (for example, $r^2 = 0.66$, $p < 0.001$, at Kota Bharu), typical of regions of
398 pollution outflow (e.g. Chin et al., 1994; Voulgarakis et al., 2011), this relationship is much weaker in
399 the DOE measurements ($r^2 = 0.01$, $p < 0.001$, again at Kota Bharu). This strong evidence for some
400 local influence on the measured DOE O_3 values means it is difficult to be certain of the large-scale
401 representativeness of the DOE data; we return to this point in our discussion (Section 4).

402

403 *3.5 Year-to-year variation in the influence of cold surges*

404 We have shown that both 'average' and individual cold surges have an appreciable impact on levels
405 of O_3 as well as CO in a broad area of the SCS. We now consider whether there is year-to-year
406 variability in this impact. We begin by considering V_5 in relation to ENSO (as measured by the MEI).
407 Figure 8 shows a relatively weak relationship ($r^2 = 0.08$, $p = 0.10$) between the seasonal mean value of
408 V_5 and the corresponding seasonal mean value of the MEI. During La Nina (negative MEI values) NH
409 winters northerly winds are, on average, stronger than in El Nino winters. The ENSO influence on
410 northerly winds increases through the season from November ($r^2 = 0.01$; $r = -0.07$) to February ($r^2 =$
411 0.21; $r = 0.46$). The overall seasonal relationship is much stronger when V_{15} is considered (seasonal r^2
412 $= 0.39$, $p < 0.001$) as are the individual monthly relationships (e.g. November $r^2 = 0.05$; February $r^2 =$
413 0.40), which, as for V_5, increase in strength through the season. This strong relation between ENSO
414 and V_{15} is consistent with the analyses of Zhang et al. (1997) which focussed on regions somewhat
415 away from the equator. So it appears northerly winds further from the equator are more influenced by
416 the ENSO state, and it follows that northerly winds closer to the equator are less variable year-to-year.

417

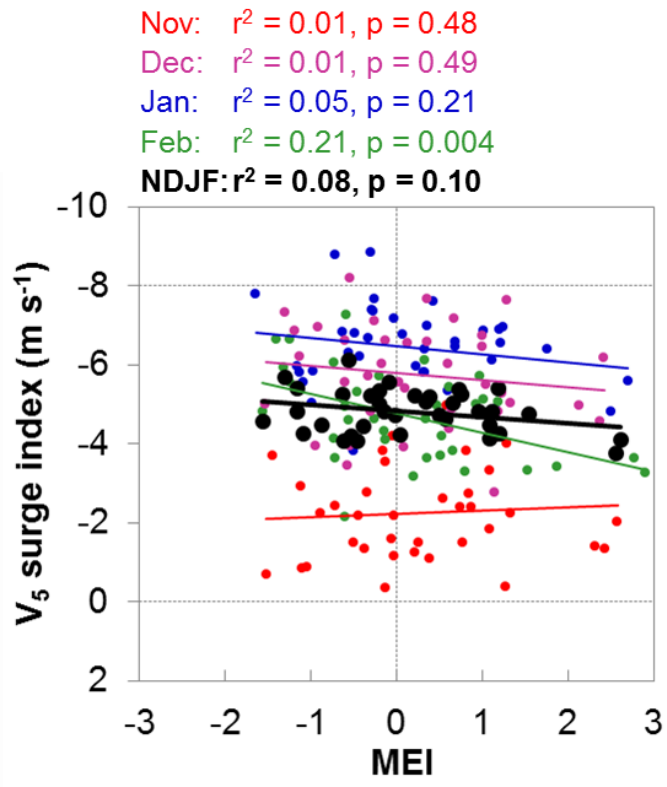

418

419 **Figure 8:** Relationship between the Multivariate ENSO Index (MEI) and the V_5 index. NDJF seasonal (black)
420 and monthly (November = red, December = purple, January = blue, February = green) mean values are presented.
421 For each line of best fit a coefficient of determination (r^2) and associated p value are given. Constructed using
422 ERA-interim data for November to February 1979-2015 (37 years, so 148 months in total) and MEI data.

423

424 Given that during NH winter 1) ENSO has some influence on monthly and seasonal mean northerly
425 winds in the SCS, and 2) the strength of northerly winds influences air quality in our study area, we
426 might also expect corresponding year-to-year variability in levels of O_3 and CO. However, with the
427 MACC Reanalysis covering a period of 10 years we have been able to define just three El Nino
428 (2004/05, 2006/07, 2009/10) and three La Nina (2007/08, 2010/11, 2011/12) NDJF seasons in our
429 analysis. This relatively short record, along with the fact that cold surges are not the only factor
430 relevant to atmospheric composition that varies with respect to ENSO, mean that the analysis in the
431 following paragraph ought to be considered an initial step towards answering this question.

432 In agreement with Figure 8, Figure 9 shows v in most of the SCS, and particularly further from the
433 equator, is stronger in La Nina winters than in El Nino winters. However, Figure 8 also suggests that
434 CO and O_3 are higher in La Nina winters only near the region over which the V_{15} index is calculated.

In most other parts of SE Asia pollutant levels are higher during El Nino winters. For example, Figure 9 shows elevated CO over Sumatra which is an indicator of landscape fires that, although more frequent from June-October (Reid et al., 2012), can occur during the NEM season (e.g. during February 2005 and November 2006). This analysis suggests that, while perceptible, year-to-year variations in cold surge activity are not the dominant influence of ENSO on atmospheric composition in most of this region during NDJF. Conversely, it is also worth noting that landscape fires occurring during El Nino NH winters can partly obscure the role of cold surges (e.g. in our analysis in Figure 3). If we repeat that analysis but exclude the winters of 2004/05 and 2006/07 (where, as noted above, there were significant fires in Sumatra) then the pollution anomaly – particularly for CO – associated with strong northerly winds is further enhanced just south of the equator (not shown).

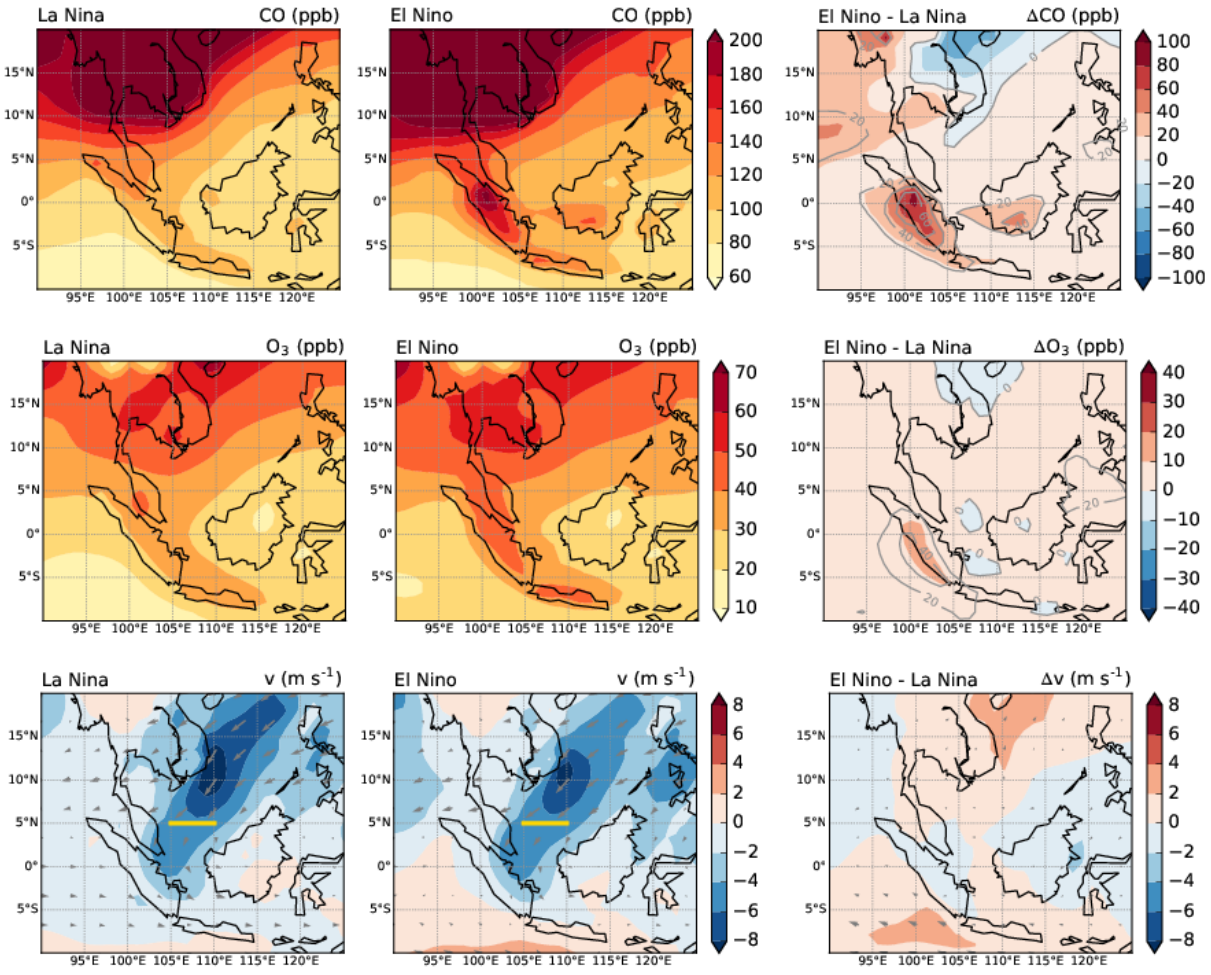

Figure 9: Composites for La Nina (left) and El Nino (centre) and the difference between the two (right) for CO (top), O_3 (middle) and v (bottom). The line over which V_5 is calculated is marked in gold in the v panels. In the difference plots the shading shows absolute differences, and the labelled grey contours show percentage differences. Composites for El Nino and La Nina were constructed from, respectively, the three highest and three lowest seasonal MEI values (averaged over the October-November, November-December, December-January, and January-February values) in the nine complete NDJF seasons in the MACC Reanalysis.

4. Discussion and Conclusions

Our analysis of MACC Reanalysis data, along with the supporting trajectory calculations, has shown that NEM cold surges have a significant impact on aspects of air quality in SE Asia. The largest impact is in a region covering much of the Indochinese Peninsular and surrounding seas, where CO and O_3 are elevated by, respectively, >60% (~80 ppb) and >40% (~15 ppb), during 'average' cold surge conditions (using the V_5 definition). In much of this area, and indeed also in the wider SE Asia region, exceedances of the WHO's Air Quality Guideline value for O_3 of 50 ppb mostly occur during cold surge periods. It is of interest to compare these results with studies examining the influence of pollution originating in East Asia on O_3 in North America. For example, Zhang et al. (2008) diagnosed a ground-level O_3 enhancement due to Asian pollution, covering most of the western half of continental USA during NH spring, of 5-7 ppb. For the same season and region, Lin et al. (2012) found that Asian pollution contributed 8-15 ppb on days when surface O_3 exceeded 60 ppb. As such, the seasonal influence of East Asian pollution on air quality in Southeast Asia could be at least as large as the corresponding, well-studied influence on North America. Zhang et al. (2008), and later both Cooper et al. (2010) and Lin et al. (2017), also demonstrated a growing influence of East Asian pollution on O_3 in North America. It seems reasonable to speculate that a similar trend will have affected our region of study. Zhang et al. (2016) showed large increases in O_3 over SE Asia between 1980-2010, but did not explore the details of pollution transport within the region in different seasons. Within this work, it is difficult to demonstrate conclusive evidence for such trends because 1) our ten year analysis period is shorter than ideal for this type of investigation, and 2) some potentially complicating discontinuities exist within the MACC Reanalysis (see Inness et al., 2013; Bocquet et al., 2015). Detailed studies with chemical transport models will help to isolate the importance of East

476 Asian pollution for this region, as well as to examine the relative impact of changes in East Asian
477 pollutant emissions and changes in regional circulation patterns (e.g. Cai et al., 2017).

478 We also showed that available O_3 observations at DOE surface sites on the east coast of Peninsular
479 Malaysia and equivalent MACC Reanalysis data exhibit similar day-to-day variability, linked to cold
480 surges, but that measured O_3 levels are typically lower. The measured levels of CO and nitrogen
481 oxides and their correlations with O_3 are indicative of a competing influence from local urban
482 pollution, and suggest that it is difficult to be certain of the large-scale representativeness of the DOE
483 data. Comprehensive surface observations from a truly 'background' site would therefore be
484 extremely desirable for studying the impact of long-range transport of pollution in cold surges on
485 atmospheric composition in SE Asia. Indeed, Sofen et al. (2016) suggest that for O_3, this region –
486 typical of tropical areas – is not characterised at all by existing measurement sites. One candidate is
487 the research station established recently by the University of Malaya at Bachok, a rural area on the
488 coast 25 km southeast of the Kota Bharu site considered here, which Oram et al. (unpublished results)
489 show is subject to appreciable pollution from East Asia during cold surges. The physical properties of
490 the lower atmosphere (e.g. the mixing height) at sites in this region are modified by cold surges (e.g.
491 Samah et al., 2016), and the importance of these modifications for atmospheric composition needs to
492 be understood. Further, any coastal site in this region is likely to be strongly affected by diurnal sea
493 breeze circulations (see Qian et al., 2013), and indeed Dominick et al. (2015) have shown that this
494 type of circulation could be important in controlling particulate matter concentrations at the Bachok
495 site. These points, along with rapid regional urbanization (Schneider et al., 2015) in largely coastal
496 cities, encourages further examination of coastal processes in the tropics related to air quality, which
497 are not likely to be fully captured in a relatively coarse resolution product such as the MACC
498 Reanalysis employed here.

499 In agreement with past studies (e.g. Zhang et al., 1997) we found year-to-year variations in cold surge
500 activity linked to ENSO. In our analysis the relationship between ENSO and meridional wind was
501 stronger further from the equator and later in the season. However, our analysis also shows that
502 variations in cold surge activity do not appear to be the dominant influence of ENSO on atmospheric

composition in most of the region. Instead, changes in emissions from fires, known to be influenced by ENSO-related variations in regional climate, appear to be more important (e.g. Reid et al., 2012; Inness et al., 2015; Voulgarakis et al., 2015).

Though we have mostly focussed on variations in O_3, cold surges also clearly lead to significant enhancements in CO (e.g. Figure 3), a gas with industrial sources that is known to be well correlated with a range of other anthropogenic pollutants (e.g. Shao et al., 2011). For some gases, such as chlorinated very short-lived substances (e.g. dichloromethane, CH_2Cl_2) that have the potential to contribute to stratospheric O_3 depletion, the pollutant source distribution is likely to be more dominated by the mid-latitudes than is the case for CO, and so the signature of NEM cold surges on this aspect of atmospheric composition in SE Asia will be proportionately larger. Measurements of a wider range of anthropogenically influenced gases in this season and region will therefore be of great interest.

Acknowledgments

This research was supported by NERC International Opportunities Fund project NE/J016012/1. We acknowledge use of the NAME atmospheric dispersion model and associated NWP meteorological data sets made available to us by the UK Met Office. We also acknowledge the significant storage resources and analysis facilities made available to us on JASMIN by STFC CEDA along with the corresponding support teams. We are grateful for use of data provided by the MACC-II project, funded by the European Union under the 7th Framework Programme. We also thank the Malaysian Department of Environment for providing the air quality observations. The constructive comments of two anonymous reviewers and Mr Ooi See Hai (University of Malaya) are also gratefully acknowledged.

References

Ashfold, M. J.; Pyle, J. A.; Robinson, A. D.; Meneguz, E.; Nadzir, M. S. M.; Phang, S. M.; Samah, A. A.; Ong, S.; Ung, H. E.; Peng, L. K.; Yong, S. E. & Harris, N. R. P. Rapid transport of East Asian pollution to the deep tropics. Atmospheric Chemistry and Physics, 2015, 15, 3565-3573.

ASMA, Standard Operating Procedure for Continuous Air Quality Monitoring. Selangor: Alam Sekitar Sdn. Bhd. Shah Alam; 2007.

Bocquet, M.; Elbern, H.; Eskes, H.; Hirtl, M.; Žabkar, R.; Carmichael, G. R.; Flemming, J.; Inness, A.; Pagowski, M.; Pérez Camaño, J. L.; Saide, P. E.; San Jose, R.; Sofiev, M.; Vira, J.; Baklanov, A.; Carnevale, C.; Grell, G. & Seigneur, C. Data assimilation in atmospheric chemistry models: current status and future prospects for coupled chemistry meteorology models. Atmospheric Chemistry and Physics, 2015, 15, 5325-5358.

Cai, W.; Li, K.; Liao, H.; Wang, H. & Wu, L. Weather conditions conducive to Beijing severe haze more frequent under climate change. Nature Climate Change, 2017, 7, 257-262.

Chang, C.-P.; Erickson, J. E. & Lau, K. M. Northeasterly Cold Surges and Near-Equatorial Disturbances over the Winter MONEX Area during December 1974. Part I: Synoptic Aspects. Monthly Weather Review, 1979, 107, 812-829.

Chang, C.-P.; Harr, P. A. & Chen, H.-J. Synoptic Disturbances over the Equatorial South China Sea and Western Maritime Continent during Boreal Winter. Monthly Weather Review, 2005, 133, 489-503.

Chin, M.; Jacob, D. J.; Munger, J. W.; Parrish, D. D. & Doddridge, B. G. Relationship of ozone and carbon monoxide over North America. Journal of Geophysical Research, 1994, 99, 14565-14573.

Cooper, O. R.; Parrish, D. D.; Stohl, A.; Trainer, M.; Nedelec, P.; Thouret, V.; Cammas, J. P.; Oltmans, S. J.; Johnson, B. J.; Tarasick, D.; Leblanc, T.; McDermid, I. S.; Jaffe, D.; Gao, R.; Stith, J.; Ryerson, T.; Aikin, K.; Campos, T.; Weinheimer, A. & Avery, M. A. Increasing springtime ozone mixing ratios in the free troposphere over western North America. Nature, 2010, 463, 344-348.

Dee, D. P.; Uppala, S. M.; Simmons, A. J.; Berrisford, P.; Poli, P.; Kobayashi, S.; Andrae, U.; Balmaseda, M. A.; Balsamo, G.; Bauer, P.; Bechtold, P.; Beljaars, A. C. M.; van de Berg, L.; Bidlot, J.; Bormann, N.; Delsol, C.; Dragani, R.; Fuentes, M.; Geer, A. J.; Haimberger, L.; Healy, S. B.; Hersbach, H.; Hólm, E. V.; Isaksen, L.; Kållberg, P.; Köhler, M.; Matricardi, M.; McNally, A. P.; Monge-Sanz, B. M.; Morcrette, J.-J.; Park, B.-K.; Peubey, C.; de Rosnay, P.; Tavolato, C.; Thépaut, J.-N. & Vitart, F. The ERA-Interim reanalysis: configuration and performance of the data assimilation system. Quarterly Journal of the Royal Meteorological Society, 2011, 137, 553-597.

Dominick, D.; Latif, M. T.; Juneng, L.; Khan, M. F.; Amil, N.; Mead, M. I.; Nadzir, M. S. M.; Moi, P. S.; Samah, A. A.; Ashfold, M. J.; Sturges, W. T.; Harris, N. R. P..; Robinson, A. D. & Pyle, J. A. Characterisation of particle mass and number concentration on the east coast of the Malaysian Peninsula during the northeast monsoon. Atmospheric Environment, 2015, 117, 187-199.

Hai, O. S.; Samah, A. A.; Chenoli, S. N.; Subramaniam, K. & Ahmad Mazuki, M. Y. Extreme Rainstorms that Caused Devastating Flooding across the East Coast of Peninsular Malaysia during November and December 2014. Weather and Forecasting, 2017, 32, 849-872.

Hou, X.; Zhu, B.; Fei, D.; Zhu, X.; Kang, H. & Wang, D. Simulation of tropical tropospheric ozone variation from 1982 to 2010: The meteorological impact of two types of ENSO event Journal of Geophysical Research: Atmospheres, 2016, 121, 9220-9236.

Huang, W.-R.; Wang, S.-Y. & Chan, J. C. L. Discrepancies between global reanalyses and observations in the interdecadal variations of Southeast Asian cold surge International Journal Of Climatology, 2011, 31, 2272-2280.

Inness, A.; Baier, F.; Benedetti, A.; Bouarar, I.; Chabrillat, S.; Clark, H.; Clerbaux, C.; Coheur, P.; Engelen, R. J.; Errera, Q.; Flemming, J.; George, M.; Granier, C.; Hadji-Lazaro, J.; Huijnen, V.; Hurtmans, D.; Jones, L.; Kaiser, J. W.; Kapsomenakis, J.; Lefever, K.; Leitão, J.; Razinger, M.; Richter, A.; Schultz, M. G.; Simmons, A. J.; Suttie, M.; Stein, O.; Thépaut, J.-N.; Thouret, V.; Vrekoussis, M.; Zerefos, C. & the MACC team. The MACC reanalysis: an 8 yr data set of atmospheric composition. Atmospheric Chemistry and Physics, 2013, 13, 4073-4109.

Inness, A.; Benedetti, A.; Flemming, J.; Huijnen, V.; Kaiser, J. W.; Parrington, M. & Remy, S. The ENSO signal in atmospheric composition fields: emission-driven versus dynamically induced changes. Atmospheric Chemistry and Physics, 2015, 15, 9083-9097.

Jones, A.; Thomson, D.; Hort, M. & Devenish, B. The U.K. Met Office's Next-Generation Atmospheric Dispersion Model, NAME III. Air Pollution Modeling and Its Application XVII, Borrego, C. & Norman, A.-L. (Eds.), Springer US, 2007, 580-589.

Juneng, L. & Tangang, F. T. Long-term trends of winter monsoon synoptic circulations over the maritime continent: 1962—2007. Atmospheric Science Letters, 2010, 11, 199-203.

Latif, M. T.; Huey, L. S. & Juneng, L. Variations of surface ozone concentration across the Klang Valley, Malaysia. Atmospheric Environment, 2012, 61, 434 - 445

Latif, M. T.; Dominick, D.; Ahamad, F.; Khan, M. F.; Juneng, L.; Hamzah, F. M. & Nadzir, M. S. M. Long term assessment of air quality from a background station on the Malaysian Peninsula. Science of The Total Environment, 2014, 482-483, 336-348.

Latif, M. T.; Dominick, D.; Ahamad, F.; Ahamad, N. S.; Khan, M. F.; Juneng, L.; Xiang, C. J.; Nadzir, M. S. M.; Robinson, A. D.; Ismail, M.; Mead, M. I. & Harris, N. R. P. Seasonal and long term variations of surface ozone concentrations in Malaysian Borneo. Science of The Total Environment, 2016, 573, 494-504.

Lelieveld, J.; Evans, J. S.; Fnais, M.; Giannadaki, D. & Pozzer, A. The contribution of outdoor air pollution sources to premature mortality on a global scale. Nature, 2015, 525, 367-371.

Lin, M.; Fiore, A. M.; Horowitz, L. W.; Cooper, O. R.; Naik, V.; Holloway, J.; Johnson, B. J.; Middlebrook, A. M.; Oltmans, S. J.; Pollack, I. B.; Ryerson, T. B.; Warner, J. X.; Wiedinmyer, C.; Wilson, J. & Wyman, B. Transport of Asian ozone pollution into surface air over the western United States in spring. Journal of Geophysical Research, 2012, 117.

Lin, M.; Horowitz, L. W.; Oltmans, S. J.; Fiore, A. M. & Fan, S. Tropospheric ozone trends at Mauna Loa Observatory tied to decadal climate variability. Nature Geoscience, 2014, 7, 136-143.

Lin, M.; Horowitz, L. W.; Payton, R.; Fiore, A. M. & Tonnesen, G. US surface ozone trends and extremes from 1980 to 2014: quantifying the roles of rising Asian emissions, domestic controls, wildfires, and climate. Atmospheric Chemistry and Physics, 2017, 17, 2943-2970.

608 Liu, H.; Jacob, D. J.; Bey, I.; Yantosca, R. M.; Duncan, B. N. & Sachse, G. W. Transport pathways
609 for Asian pollution outflow over the Pacific: Interannual and seasonal variations. Journal Of
610 Geophysical Research, 2003, 108, 8786.

611 Morrison, N. L. & Webster, H. N. An Assessment of Turbulence Profiles in Rural and Urban
612 Environments Using Local Measurements and Numerical Weather Prediction Results. Boundary-
613 Layer Meteorology, 2005, 115, 223-239.

614 Oman, L. D.; Ziemke, J. R.; Douglass, A. R.; Waugh, D. W.; Lang, C.; Rodriguez, J. M. & Nielsen, J.
615 E. The response of tropical tropospheric ozone to ENSO. Geophysical Research Letters, 2011, 38,
616 L13706.

617 Ooi, S. H.; Samah, A. A. & Braesicke, P. A case study of the Borneo Vortex genesis and its
618 interactions with the global circulation. Journal Of Geophysical Research, 2011, 116, D21116.

619 Oram, D. E.; Ashfold, M. J.; Laube, J. C.; Gooch, L. J.; Humphrey, S.; Sturges, W. T.; Leedham-
620 Elvidge, E.; Forster, G. L.; Harris, N. R. P.; Mead, M. I.; Samah, A. A.; Phang, S. M.; Ou-Yang, C.-
621 F.; Lin, N.-H.; Wang, J.-L.; Baker, A. K.; Brenninkmeijer, C. A. M.; Sherry, D. A growing threat to
622 the ozone layer from short-lived anthropogenic chlorocarbons. Atmospheric Chemistry and Physics
623 Discussions, in review, 2017, 1-20, doi:10.5194/acp-2017-497.

624 Qian, J.-H.; Robertson, A. W. & Moron, V. Diurnal Cycle in Different Weather Regimes and Rainfall
625 Variability over Borneo Associated with ENSO. Journal Of Climate, 2013, 26, 1772-1790.

626 Reid, J. S.; Xian, P.; Hyer, E. J.; Flatau, M. K.; Ramirez, E. M.; Turk, F. J.; Sampson, C. R.; Zhang,
627 C.; Fukada, E. M. & Maloney, E. D. Multi-scale meteorological conceptual analysis of observed
628 active fire hotspot activity and smoke optical depth in the Maritime Continent. Atmospheric
629 Chemistry and Physics, 2012, 12, 2117-2147.

630 Reid, J. S.; Hyer, E. J.; Johnson, R. S.; Holben, B. N.; Yokelson, R. J.; Zhang, J.; Campbell, J. R.;
631 Christopher, S. A.; Di Girolamo, L.; Giglio, L.; Holz, R. E.; Kearney, C.; Miettinen, J.; Reid, E. A.;
632 Turk, F. J.; Wang, J.; Xian, P.; Zhao, G.; Balasubramanian, R.; Chew, B. N.; Janjai, S.; Lagrosas, N.;
633 Lestari, P.; Lin, N.-H.; Mahmud, M.; Nguyen, A. X.; Norris, B.; Oanh, N. T.; Oo, M.; Salinas, S. V.;
634 Welton, E. J. & Liew, S. C. Observing and understanding the Southeast Asian aerosol system by
635 remote sensing: An initial review and analysis for the Seven Southeast Asian Studies (7SEAS)
636 program. Atmospheric Research, 2013, 122, 403-468.

637 Samah, A. A.; Babu, C.; Varikoden, H.; Jayakrishnan, P. & Hai, O. S. Thermodynamic and dynamic
638 structure of atmosphere over the east coast of Peninsular Malaysia during the passage of a cold surge.
639 Journal of Atmospheric and Solar-Terrestrial Physics, 2016, 146, 58-68.

640 Schneider, A.; Mertes, C. M.; Tatem, A. J.; Tan, B.; Sulla-Menashe, D.; Graves, S. J.; Patel, N. N.;
641 Horton, J. A.; Gaughan, A. E.; Rollo, J. T.; Schelly, I. H.; Stevens, F. R. & Dastur, A. A new urban
642 landscape in East-Southeast Asia, 2000-2010. Environmental Research Letters, 2015, 10, 034002.

643 Shao, M.; Huang, D.; Gu, D.; Lu, S.; Chang, C. & Wang, J. Estimate of anthropogenic halocarbon
644 emission based on measured ratio relative to CO in the Pearl River Delta region, China. Atmospheric
645 Chemistry and Physics, 2011, 11, 5011-5025.

646 Sheel, V.; Sahu, L. K.; Kajino, M.; Deushi, M.; Stein, O. & Nedelec, P. Seasonal and interannual
647 variability of carbon monoxide based on MOZAIC observations, MACC reanalysis, and model
648 simulations over an urban site in India. Journal of Geophysical Research: Atmospheres, 2014,
649 2013JD021425.

650 Silva, R. A.; West, J. J.; Lamarque, J.-F.; Shindell, D. T.; Collins, W. J.; Dalsoren, S.; Faluvegi, G.;
651 Folberth, G.; Horowitz, L. W.; Nagashima, T.; Naik, V.; Rumbold, S. T.; Sudo, K.; Takemura, T.;
652 Bergmann, D.; Cameron-Smith, P.; Cionni, I.; Doherty, R. M.; Eyring, V.; Josse, B.; MacKenzie, I.
653 A.; Plummer, D.; Righi, M.; Stevenson, D. S.; Strode, S.; Szopa, S. & Zengast, G. The effect of future
654 ambient air pollution on human premature mortality to 2100 using output from the ACCMIP model
655 ensemble. Atmospheric Chemistry and Physics, 2016, 16, 9847-9862.

656 Sofen, E. D.; Bowdalo, D. & Evans, M. J. How to most effectively expand the global surface ozone
657 observing network. Atmospheric Chemistry and Physics, 2016, 16, 1445-1457.

658 Stein, O.; Schultz, M. G.; Bouarar, I.; Clark, H.; Huijnen, V.; Gaudel, A.; George, M. & Clerbaux, C.
659 On the wintertime low bias of Northern Hemisphere carbon monoxide found in global model
660 simulations. Atmospheric Chemistry and Physics, 2014, 14, 9295-9316.

661 Verstraeten, W. W.; Neu, J. L.; Williams, J. E.; Bowman, K. W.; Worden, J. R. & Boersma, K. F.
662 Rapid increases in tropospheric ozone production and export from China. Nature Geoscience, 2015, 8,
663 690-695.

664 Voulgarakis, A.; Telford, P. J.; Aghedo, A. M.; Braesicke, P.; Faluvegi, G.; Abraham, N. L.;
665 Bowman, K. W.; Pyle, J. A. & Shindell, D. T. Global multi-year O_3-CO correlation patterns from
666 models and TES satellite observations. Atmospheric Chemistry and Physics, 2011, 11, 5819-5838.

667 Voulgarakis, A.; Marlier, M. E.; Faluvegi, G.; Shindell, D. T.; Tsigaridis, K. & Mangeon, S.
668 Interannual variability of tropospheric trace gases and aerosols: The role of biomass burning
669 emissions. Journal of Geophysical Research: Atmospheres, 2015, 120, 7157-7173.

670 Wang, Z.; Liu, X. & Xie, X. Effects of Strong East Asian Cold Surges on Improving the Air Quality
671 over Mainland China. Atmosphere, 2016, 7, 38.

672 Wild, O. & Akimoto, H. Intercontinental transport of ozone and its precursors in a three-dimensional
673 global CTM. Journal of Geophysical Research: Atmospheres, 2001, 106, 27729-27744.

674 Wolter, K. & Timlin, M. S. Measuring the strength of ENSO events: How does 1997/98 rank?
675 Weather, 1998, 53, 315-324.

676 Zhang, Y.; Sperber, K. R. & Boyle, J. S. Climatology and Interannual Variation of the East Asian
677 Winter Monsoon: Results from the 1979-95 NCEP/NCAR Reanalysis. Monthly Weather Review,
678 1997, 125, 2605-2619.

679 Zhang, L.; Jacob, D. J.; Boersma, K. F.; Jaffe, D. A.; Olson, J. R.; Bowman, K. W.; Worden, J. R.;
680 Thompson, A. M.; Avery, M. A.; Cohen, R. C.; Dibb, J. E.; Flock, F. M.; Fuelberg, H. E.; Huey, L.
681 G.; McMillan, W. W.; Singh, H. B. & Weinheimer, A. J. Transpacific transport of ozone pollution
682 and the effect of recent Asian emission increases on air quality in North America: an integrated
683 analysis using satellite, aircraft, ozonesonde, and surface observations. Atmospheric Chemistry and
684 Physics, 2008, 8, 6117-6136.

685 Zhang, Y.; Cooper, O. R.; Gaudel, A.; Thompson, A. M.; Nedelec, P.; Ogino, S.-Y. & West, J. J.
686 Tropospheric ozone change from 1980 to 2010 dominated by equatorward redistribution of emissions.
687 Nature Geoscience, 2016, 9, 875-879.

688 Ziemke, J. R.; Douglass, A. R.; Oman, L. D.; Strahan, S. E. & Duncan, B. N. Tropospheric ozone
689 variability in the tropics from ENSO to MJO and shorter timescales. Atmospheric Chemistry and
690 Physics, 2015, 15, 8037-8049.